Paper Number 01ICES-2327

Neutron Environment Calculations for Low Earth Orbit

M. S. Clowdsley, J. W. Wilson, J. L. Shinn
NASA Langley Research Center, Hampton, VA

F. F. Badavi
Christopher Newport University, Newport News, VA

J. H. Heinbockel
Old Dominion University, Norfolk, VA

W. Atwell
Boeing North American, Inc., Houston, TX

ABSTRACT

The long term exposure of astronauts on the developing International Space Station (ISS) requires an accurate knowledge of the internal exposure environment for human risk assessment and other onboard processes. The natural environment is moderated by the solar wind, which varies over the solar cycle. The HZETRN high charge and energy transport code developed at NASA Langley Research Center can be used to evaluate the neutron environment on ISS. A time dependent model for the ambient environment in low earth orbit is used. This model includes GCR radiation moderated by the Earth's magnetic field, trapped protons, and a recently completed model of the albedo neutron environment formed through the interaction of galactic cosmic rays with the Earth's atmosphere. Using this code, the neutron environments for space shuttle missions were calculated and comparisons were made to measurements by the Johnson Space Center with onboard detectors. The models discussed herein are being developed to evaluate the natural and induced environment data for the Intelligence Synthesis Environment Project and eventual use in spacecraft optimization.

INTRODUCTION

The commitment of astronauts to long term exposure to the space environment on the International Space Station (ISS) requires resolution of issues concerning ionizing radiation. For this reason the Intelligence Synthesis Environment (ISE) Project in collaboration with the High Performance Computation and Communication (HPCC) Project are developing visual methods for the study and optimization of the ISS radiation fields, validating these methods with data from past Shuttle flights, and planning for future multidisciplinary design optimization of the Second Generation Reusable Launch Vehicle (RLV) using multifunctional design techniques. Such methods are seen to be the primary means to reduce the impact of radiation protection requirements on mission costs. These methods will have a large impact on future missions outside of the Earth's protective magnetic field as well.

For the high inclination of the ISS (51.6^{o}), computational models indicate that about half of the ionizing radiation exposure near solar minimum results from Galactic Cosmic Rays (GCR, 233 μSv/d) and the bulk of the remainder from trapped particles (166 μSv/d, [1]). There is of course contributions from the neutron albedo of 25 to 54 μSv/d (varies with solar cycle) excluding effects of intervening material [2]. Within the spacecraft, the environment is a complex mixture of surviving primary particles and secondary radiations produced in the spacecraft structure. Various arrangements of detectors have been used to study the composition of the internal radiation fields within spacecrafts in low Earth orbit (LEO) [3-6]. These studies need to be understood in terms of computational models [7-9] to allow a better understanding of the local environment of the astronauts' critical tissues in addition to aiding future design processes.

Measurements of neutrons on Cosmos-2044 flown at 82^{o} inclination between 216-296 km resulted in 35 μSv/d using nuclear emulsion [3] and compared favorably with the neutron albedo model of 25 μSv/d estimated for near polar orbits at the cycle 20 solar minimum [2]. Similar measurements within the Spacehab on STS-57 in a 28.5^{o} inclination orbit at 462 km yield 174 μSv/d compared to 12.5 μSv/d from the albedo neutrons near solar maximum. Unlike the Cosmos-2044 spacecraft, the Shuttle is itself a strong source of neutrons especially within the massive Spacehab module in the Shuttle bay.

Indeed, time resolved neutron measurements on the Mir and Salyut stations [10] reveal strong neutron levels mainly within the South Atlantic Anomaly (SAA) passage through the trapped proton belt against a lower background of neutrons in the remainder of time outside the SAA.

Neutron measurements using Bonner spheres and activation foils were made [4] near solar maximum in the low inclination (28.5^o) with high altitude (617 km) flight STS-31 in April 1990 and in the high inclination (62^o) with low altitude (246 km) flight STS-36 in February 1990. The neutron dose equivalent on STS-36 was found to be 45 μSv/d compared to 25 μSv/d from the albedo model and on STS-31 the measurements were 345 μSv/d compared to 12.5 μSv/d from the albedo model again showing the Shuttle to be a strong source of neutrons. Small spacecraft have relatively few locally produced neutrons as seen on Cosmos-2044 and also on the Orbiting Geophysical Observatory (OGO-6) satellite where only 3 to 4 percent corrections of the albedo neutron measurements resulted from neutrons produced locally in the spacecraft materials [3,11].

In earlier work, we had compared computational models with high LET event rates causing upsets on the Shuttle computers [7], with CR-39 measurements on the Spacehab mission D1 [12], with spectral measurements using a particle identification spectrometer telescope [8], and with time resolved lineal energy distributions in tissue equivalent proportional counters (TEPCs, [9]). It was found in these studies that the details of the vehicle geometry and materials as well as the detector response were required to be accurately modeled in order to relate the measured data to computed instrument responses based on computer evaluated flux at the detector location within the vehicle. Over-simplification of the details would usually result in poor comparisons. Through these comparisons, two weaknesses in the codes were identified as lack of a description of meson production [7] and the lack of an adequate low energy neutron transport algorithm compatible with the HZETRN shielding code [13-15]. Most of these results are determined by the charged particle environment except for the TEPC which is equally sensitive to neutrons and photons. Still there is great advantage in terms of code testing to evaluate the codes against measurements sensitive only (or primarily) to the neutron environment. In making such comparisons, we first need an improved description of the trapped proton environment and the albedo neutron environment which make non-negligible contribution to the total environment in LEO. In the present paper we will present improved trapped radiation and albedo neutron environmental models, evaluate the total environment within the specific locations of the Shuttle and compare with measured neutrons on specific Shuttle missions.

MODELS OF THE NATURAL ENVIRONMENT

There are three sources of particles in the LEO environment considered herein: galactic cosmic rays (GCR), particles trapped in the Earth's magnetic field, and neutrons produced as secondaries in interaction of the GCR with the Earth's atmosphere. The "splash" electrons and protons are secondary particles produced in the atmosphere and are of energy too low to escape the geomagnetic field. These "splash" particles follow the geomagnetic field lines to the mirror point where they re-enter the atmosphere. These splash particles are of low intensity and are not treated herein. The particle fields are all modulated (represented by sunspot number, SSN) through the solar cycle through various mechanisms. Near term ISS missions will be near solar maximum as shown in figure 1.

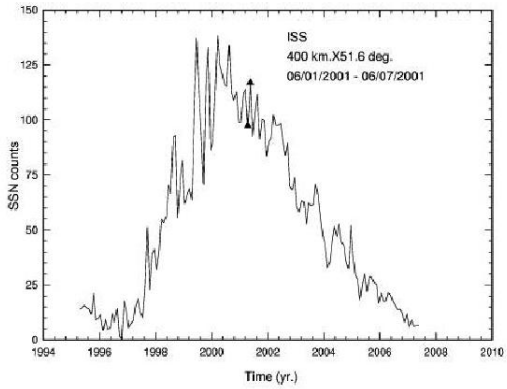

Fig. 1 Projected sunspot number showing time of a Shuttle mission to ISS in June 2001.

GALACTIC COSMIC RAYS - The GCR are represented by the environments evaluated by Badhwar and O'Neill [16] for successive solar minima and maxima and interpolated herein according to the Deep River Neutron Monitor (DRNM, [17]). The variation of the DRNM over the present solar cycle with future projections is shown in figure 2. DRNM variations in future years are extrapolated according to correlations with the projected sunspot number (SSN) in figure 1. The Badhwar/O'Neill model is interpolated according to the smoothed sunspot numbers and at successive maxima and minima of the DRNM correlation functions [17]. The Smart and Shea [18] vertical cutoff rigidities (scaled in altitude) are used to calculate the orbit averaged geomagnetic transmission factors including the effects of the Earth's shadow. The ISS GCR environment near the present solar maximum is shown in figure 3 during geomagnetic quite times during the first week of June of 2001. The delay as the modulation zone is filled by the solar wind is apparent by the time delay to GCR minimum.

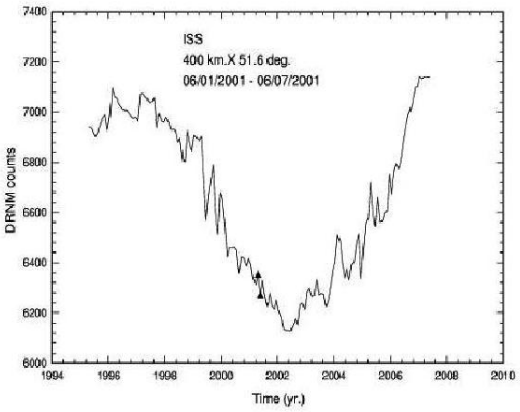

Fig. 2 Projected galactic cosmic ray levels as Deep River Neutron Monitor count rate.

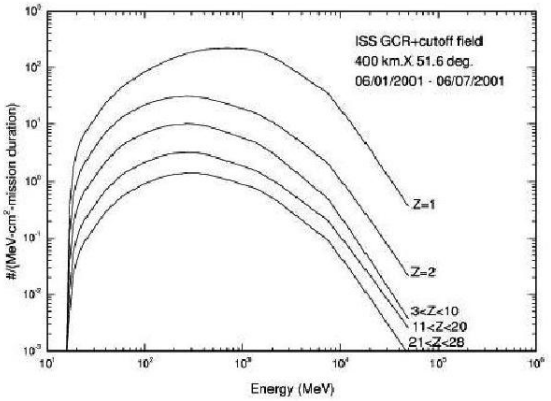

Fig. 3 GCR environment in ISS orbit for June 2001.

TRAPPED PROTONS - The trapped radiations consist of two populations. The inner zone particles result from the decay of atmospheric neutrons as they leak from the Earth's atmosphere into the trapping region. The inner zone particles are lost from the trapping region by interaction with the tenuous atmosphere and generally have long trapping lifetimes. The inner zone consists of both proton and electron decay products. The outer zone consists of electrons which are not really trapped but are continuously injected into the magnetospheric tail region and radially diffuse to lower altitudes until they are lost in the atmosphere near the polar regions. These outer zone electrons form the well known aurora during geomagnetic disturbances. The average kinetic energy of either the outer or inner zone electrons is a few hundred keV. These electrons are easily removed by the slightest amount of shielding and are mainly of concern to an astronaut in a spacesuit. Within any pressure vessel such as Shuttle or ISS, electrons are easily eliminated by the meteoroid bumper and pressure vessel. Only the protons with energies near or above the hundred MeV range are of concern within the Shuttle or ISS.

The particles trapped in the geomagnetic field were modeled from data obtained during two epochs of solar cycle 20 (solar minimum of 1964 and solar maximum of 1970) and best estimates of magnetic field coordinates were taken from current field models at the time of measurement [19]. The 1964 analysis using the magnetic field model IGRF-65/epoch 1964 resulted in particle population maps AP8 MIN and AE8 MIN for trapped protons and electrons respectively. The 1970 analysis using the magnetic field model US C&GS/epoch 1970 resulted in the particle population maps of AP8 MAX and AE8 MAX. The proton environment has as its source the neutron albedo and the losses occur through atmospheric interaction.

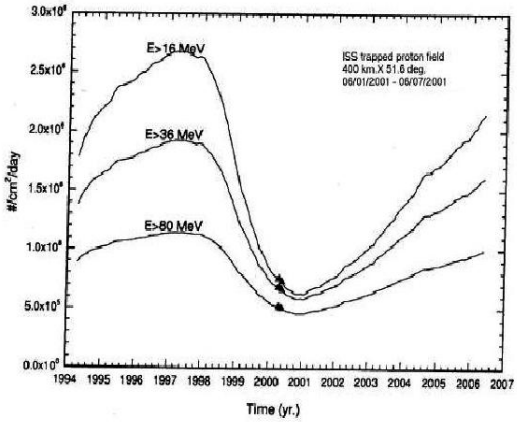

Fig. 4. Trapped proton environment projected for a mission to ISS in June 2001.

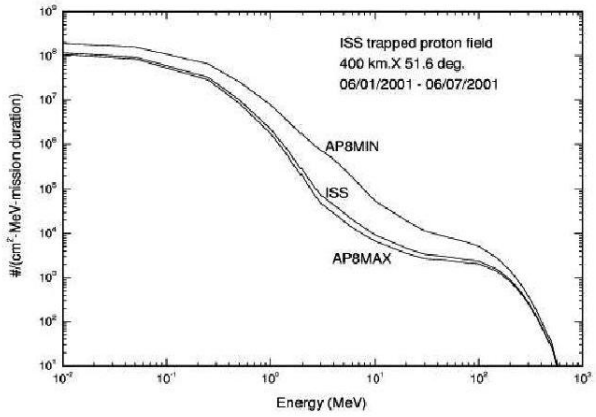

Fig. 5. Trapped proton environment projected fo a mission to ISS in June 2001 with AP8MAX/MIN environmental models.

The proton environment is then proportional, in steady state, to the source and the lifetime due to atmospheric interaction [20]. The interpolation procedure assumes a steady state solution to the population kinetic equations as the product of the albedo neutron source and the lifetimes which is proportional to the product of neutron monitor count rate and solar radio output at the 10.7 cm. The proton flux is then extrapolated using the above

assumptions. The proton flux is assumed to depend on the prior 15 month average of the Deep River Neutron Monitor count rate times the radio flux output with exponential dependence [17]. The results are shown in figure 4 near the current solar maximum. The proton flux is shown for comparison with AP8 MIN and AP8 MAX in figure 5. The current model is within 20 to 30 percent of the values given by NOAAPRO [21].

NEUTRON ALBEDO – Abedo neutrons result from the interaction of cosmic rays with the Earth's atmosphere. As the cosmic ray intensities are modulated by the solar activity so are the atmospheric neutrons modulated with time. The atmospheric neutron model is a parametric fit to data gathered by the Langley Research Center studies of the radiations at SST altitudes in the years 1965 to 1971 covering the rise and decline of solar cycle 20. Scaling of the data with respect to geomagnetic cutoff, altitude, and modulation of the Deep River Neutron Monitor was found to allow mapping of the environment to all locations at all times resulting in an empirically based model for atmospheric neutrons [22]. The basic data consisted of measurements with fast neutron spectrometers encapsulated in a charged particle anticoincidence scintillator and using pulse shape discrimination to reject gamma ray counts [23]. The model was based on global surveys with airplanes and balloons. The model was scaled in terms of rigidity *R (GV)*, atmospheric depth *x(g/cm^2)*, and Deep River Neutron Monitor count rate. The resulting model is shown in figure 6 in comparison to the measurements of University of New Hampshire [11] on OGO-6.

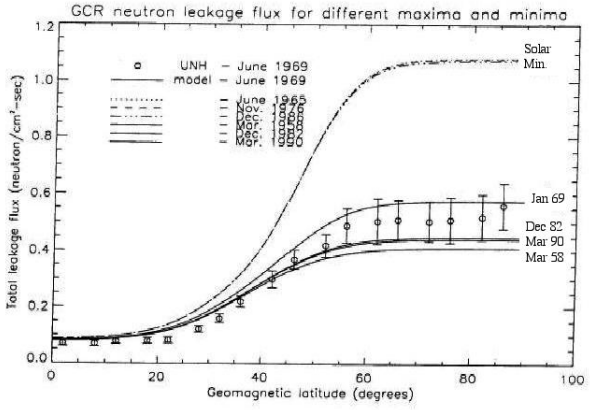

Fig. 6 LEO neutron albedo environment in comparison to the OGO-6 measurements [11].

EVALUATION OF THE INDUCED ENVIRONMENT

The charged particle environment on the Shuttle has been experimentally studied in detail using track detectors, charged particle telescopes, and tissue equivalent proportional counters providing a basis for evaluating our understanding of environmental models, transport procedures, and engineering model databases representing the distribution of Shuttle materials about the measurement locations. Good success has been achieved in predicting the internal Shuttle charged particle environmental components [7-9]. A weakness in those earlier comparisons, was the lack of attention given to the neutron component. Neutron measurements were made by Keith et al. [4] using a Bonner sphere setup on STS-31 and STS-36 which will be the focus of the present evaluation. One limitation of the measurements is the range of sizes in the Bonner sphere setup which ranged from 2 to 8 inches. The energy range is limited to below about 15 MeV neutron energies. Analysis of the measurements were through fitting a simple power law for the flux spectrum (see table 1) and is used herein as the basis of comparison.

Table 1. Space Shuttle measurements of LEO environment.

Parameter	STS-36	STS-31
Launch date	28 Feb. 90	24 Apr. 90
Duration (days)	4.43	5.05
Altitude (km)	246	617
Inclination (^{o})	62	28.5
Flux (n/cm^2 MeV min.)	$5.92(\pm 0.27)/E^{0.765}$	$45.1(\pm 1.9)/E^{0.765}$
TLD Dose (μGy/d)	89	1660

The models for the natural environment are discussed in the previous section and the induced neutron environment is evaluated using the HZETRN code with an improved neutron transport procedure and definition of the vehicle geometry. The types and energy distributions of particles transmitted through a shield material require the solution to a transport description of the process with appropriate boundary conditions related to the external space radiation environment. The relevant transport equations are the linear Boltzmann equations derived on the basis of conservation principles for the flux density $\phi_j(\boldsymbol{x},\boldsymbol{\Omega},E)$ of type j particles at location $\boldsymbol{x}$ moving in direction $\boldsymbol{\Omega}$ with energy E as

$$\boldsymbol{\Omega}\bullet\nabla\phi_j(\boldsymbol{x},\boldsymbol{\Omega},E) = \Sigma\int \sigma_{jk}(\boldsymbol{\Omega},\boldsymbol{\Omega}',E,E')\,\phi_k(\boldsymbol{x},\boldsymbol{\Omega}',E')\,d\boldsymbol{\Omega}'\,dE' - \sigma_j(E)\,\phi_j(\boldsymbol{x},\boldsymbol{\Omega},E) \quad (1)$$

where $\sigma_j(E)$, $\sigma_{jk}(\boldsymbol{\Omega},\boldsymbol{\Omega}',E,E')$ are the media macroscopic cross sections for various atomic and nuclear processes including spontaneous disintegration. Equation (1) is to be solved subject to the boundary condition

$$\phi_j(\boldsymbol{\Gamma},\boldsymbol{\Omega},E) = \Psi_j(\boldsymbol{\Omega},E) \qquad \text{where } \boldsymbol{n}\cdot\boldsymbol{\Omega} < 0 \quad (2)$$

where $\boldsymbol{\Gamma}$ denotes a point on the boundary, $\boldsymbol{n}$ is the outward directed unit normal at $\boldsymbol{\Gamma}$, and $\Psi_j(\boldsymbol{\Omega},E)$ is the

external fluence (space environment). In general, there are hundreds of particle fields $\phi_j(\boldsymbol{x},\boldsymbol{\Omega},E)$ with several thousand cross-coupling terms $\sigma_{jk}(\boldsymbol{\Omega},\boldsymbol{\Omega}',E,E')$ through the integral operator in equation (1). The total cross section $\sigma_j(E)$ with the medium for each particle type of energy E may be expanded as

$$\sigma_j(E) = \sigma_{j,at}(E) + \sigma_{j,el}(E) + \sigma_{j,r}(E) \quad (3)$$

where the first term refers to collision with atomic electrons, the second term is for elastic nuclear scattering, and the third term describes nuclear reactive processes and are ordered as $1 : 10^{-5} : 10^{-8}$. This ordering allows flexibility in expanding solutions to the Boltzmann equation as a sequence of physical perturbative approximations. Special problems arise in the perturbation approach for neutrons for which the nuclear elastic process appears as the first-order perturbation and has been the focus of recent research as described below.

The double differential particle production and fragmentation cross sections $\sigma_{jk}(\boldsymbol{\Omega},\boldsymbol{\Omega}',E,E')$ of equation (1) are separated into an isotropic contribution and a remainder as

$$\sigma = \sigma_F + \sigma_{iso} \quad (4)$$

where the remainder σ_F consists of only forward directed secondary particles and σ_{iso} is dominated by lower energy particles produced in the reaction.

The solution to equation (1) can likewise be separated into two parts for which σ_F appears only in an equation like equation (1) with solution ϕ_F and a second equation for the diffuse components in which σ_{iso} appears in equation (1) but with source terms from coupling to the ϕ_F field through σ_{iso}. The solution to equation (1) for ϕ_F can be written in operational form as

$$\phi_F = G_F \Psi_B \quad (5)$$

where Ψ_B is the inbound flux at the boundary, and G_F is the Green's function associated with σ_F which reduces to a unit operator on the boundary. We will evaluate equation (5) using the marching procedure of the HZETRN code [13].

There remains the evaluation of the remainder terms σ_{iso} of equation (1), especially the low-energy neutron transport. The remainder of equation (1) following the separation given by equation (4) is

$$\boldsymbol{\Omega}\bullet\boldsymbol{\nabla}\phi_j(\boldsymbol{x},\boldsymbol{\Omega},E) = \Sigma\int \sigma_{iso,jk}(E,E')\,\phi_k(\boldsymbol{x},\boldsymbol{\Omega}',E')\,d\boldsymbol{\Omega}'\,dE' - \sigma_j(E)\,\phi_j(\boldsymbol{x},\boldsymbol{\Omega},E) + g_j(E,\boldsymbol{x}) \quad (6)$$

where the source term $g_j(E,\boldsymbol{x})$ results from the collisional σ_{iso} source with the ϕ_F field. The charged particle fields of equation (6) can be solved analytically leaving the low-energy neutron fields to be evaluated using energy multigroup methods and approximating the integral term by a mean value theorem evaluated at a parametric energy point [14,15]. It requires a solution to a boundary value problem for the distribution of neutron sources along a 512 array of directions about each location within the vehicle where the fields are to be evaluated. This can be time consuming (few minutes per ray per evaluation point) on a serial machine when mapping the radiation environment at many locations within the human body at many locations within a complex structure such as the Shuttle, RLV, ISS, or a Mars mission vehicle or habitat. The solution methodology implies a great deal of repeated operations (for each direction) with differences only in the distribution of source terms, distances to the boundaries, and boundary conditions. This high degree of parallelism will be used within the HPCC Project to greatly speed the computation by doing all 512 directions in parallel. Other parallel operations could also be used in the solution of the ϕ_F fields solved by marching procedures but will require modifications of the HZETRN code configuration.

RESULTS FOR STS-31 AND STS-36

The flight dates and orbital parameters of STS-31 and STS-36 are given in table 1. STS-36 is seen to be a low-altitude high-inclination flight dominated by the GCR in the first quarter of 1990. The STS-31 flight was a high-altitude low-inclination flight dominated by trapped proton environment a few months later. Both flights occurred near the maximum modulation effects of the solar cycle. The GCR, trapped particles, and neutron albedo were evaluated using the models described above and transported into the Shuttle materials using the multigroup-neutron/HZETRN code.

The results for the STS-36 flight are shown in figure 7. The JSC data is the solid line extending downward from the upper left corner of the graph and terminating at 15 MeV. The neutrons induced by the trapped protons is shown as the dash-dot curve in the lower left corner of the graph and contributes little to the STS-36 environment. The albedo neutrons and their secondary neutrons are shown as the dash-double dot curve which gives a sizable contribution to the neutron environment. Most of the neutrons in STS-36 were induced by the GCR in the Shuttle materials shown as the dash curve. The total neutron fluence compares favorably with the JSC measurements.

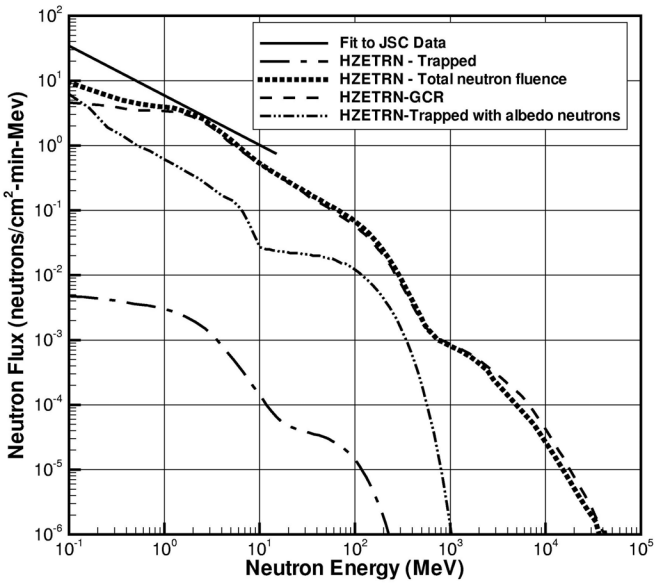

Fig. 7 The neutron environment of STS-36 (62^o inclination, 246 km) on Feb. 28 – Mar. 3, 1990 predicted by current model compared to JSC data [4].

The results for the STS-31 flight are shown in figure 8. The JSC data is again shown as the solid line extending downward from the upper left corner. In this low-inclination high-altitude mission, the neutrons induced by the trapped protons in the Shuttle materials are the dominant neutron component. Adding the albedo component makes little difference in the neutron environment. The GCR contribute neutrons at much higher energies but contribute little in the range of the measurements. The spectral shape in the important 1-10 MeV region from the neutrons induced by the trapped radiations and by the GCR are quite distinct. It is not clear if this is a limitation of the current preliminary nuclear database for developing solution methods [22] or a fundamental difference in the production processes. Also it is not clear if the spectral differences with the JSC measurements are a result of the simplified analysis of the Bonner sphere data used in reducing the measurements. An improved database is currently under development and is expected to shed more light on these issues.

CONCLUSION

Three things have been accomplished in the present activity. First, an improved description of the LEO environment has been developed in terms of time dependent trapped radiation models and an improved neutron albedo model. The second accomplishment is an improved computational procedure for evaluation of the induced neutron environment within spacecraft interiors. Finally, a step in validating the means by which we evaluate the mixed radiation environment utilizing environmental models, computational transport procedures, and vehicle geometry models has been made. Although the computational procedures for GCR components appear well represented by the JSC measurements, the trapped environment comparisons leave some open questions since the reduced spectrum from the measurements on low-inclination flight of STS-31 appears less structured than the computational model. This difference may be due the simplified analysis of the measured data or in the uncertainty in the nuclear database. These models will be used in the simulation of the radiation environments in the ISE large scale simulations of ISS and preliminary design studies of the second generation RLV.

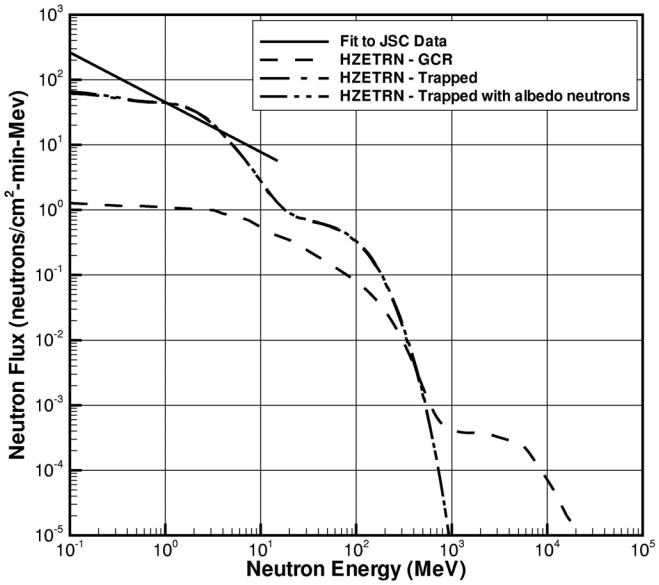

Fig. 8 The neutron environment of STS-31 (28.5^o inclination, 617 km) on Apr. 24 – 29, 1990 predicted by current model compared to JSC data [4].

REFERENCES

1. Wu, H. et al. *Estimate of Space Radiation-Induced Cancer Risks for International Space Station Orbits*. NASA TM-104818, 1996.
2. Wilson, J.W. et al. Health Phys. 57:665-668; 1989
3. Dudkin, V.E. et al. Nucl. Tracks Radiat. Meas. 20:139-141; 1992.
4. Kieth, J. E. et al. Nucl. Tracks Radiat. Meas. 20:41-47; 1992.
5. Badhwar, G.D. et al. Radiat. Meas. 24:283-289; 1995.
6. Dudkin, V.E. et al. Radiat. Meas. 25:483-484; 1995.
7. Shinn, J.L. et al. IEEE Trans. Nucl. Sci. 42:2017-2025; 1995.
8. Badhwar, G.D. et al. Radiat. Meas., 24: 129-138 1995.
9. Shinn, J.L. et al. IEEE Trans. Nucl. Sci. 45:2711-2719; 1998.
10. Lobakov, A. P. et al. Nucl. Tracks Radiat. Meas. 20:55-58; 1992.
11. Jenkins, R.W. et al. J. Geophys. Res. 76:7470-7478; 1971.
12. Weigel, B. et al. Adv. Space Res. 12: 349-354; 1992.

13. Wilson, J. W. et al. *HZETRN:Description of a free-space ion and nucleon transport and shielding computer program.* NASA TP-3495, 1995.
14. Clowdsley, M.S. et al. A comparison of the multigroup and collocation methods for solving the low-energy neutron Boltzmann equation. Can. J. Phys. 78: 45-56; 2000.
15. Clowdsley, M.S. et al. *An Improved Elastic and Nonelastic Neutron Transport Alogrithm for Space Radiation*. NASA/TP-2000-210299, 2000.
16. Badhwar, G. D. and O'Neill, P. M. Nucl. Tracks Radiat. Meas. 20: 427-410; 1995.
17. Wilson, J. W. et al. *Solar Cycle Variation and Application to the Space Radiation Environment* NASA TP-1999-209369, 1999.
18. Smart, D. F.; Shea, M. A. Geomagnetic transmission functions for 400 km altitude satellite. *18th International Cosmic Ray Conference—Conference Papers* MG Sessions, Vol. 3, Tata Inst. of Fundamental Research (Colaba, Bombay) pp. 419-422; 1983.
19. Atwell, W. et al. Space Radiation Shielding Analysis and Dosimetry for the Space Shuttle Program. In *High-Energy Radiation Background in Space,* Eds. A. C. Rester & J. I. Trombka, AIP Conference Preceedings 186, New York, 1989, pp. 289-296.
20. Blanchard R. C.; Hess, W. N. J. Geophys. Res. 69:3927; 1964.
21. Huston, S. L. et al. Adv. Space Res. 21(12):1625-1634; 1998.
22. Wilson, J.W. et al. *Transport Methods and Interactions for Space Radiations*, NASA RP-1257, 1991.
23. Korff, S.A. et al. *Atmospheric Neutrons*. NASA CR 3126, 1979.

CONTACT

m.s.clowdsley@larc.nasa.gov

John.w.wilson@larc.nasa.gov